How Robust Is the Weakening of the Pacific Walker Circulation in CMIP5 Idealized Transient Climate Simulations?

ELINA PLESCA, VERENA GRÜTZUN, AND STEFAN A. BUEHLER

Meteorological Institute, Center for Earth System Research and Sustainability, University of Hamburg, Hamburg, Germany

(Manuscript received 6 March 2017, in final form 15 September 2017)

ABSTRACT

The tropical overturning circulations are likely weakening under increased CO_2 forcing. However, insufficient understanding of the circulations' dynamics diminishes the full confidence in such a response. Based on a CMIP5 idealized climate experiment, this study investigates the changes in the Pacific Walker circulation under anthropogenic forcing and the sensitivity of its weakening response to internal variability, general circulation model (GCM) configuration, and indexing method. The sensitivity to internal variability is analyzed by using a 68-member ensemble of the MPI-ESM-LR model, and the influence of model physics is analyzed by using the 28-member CMIP5 ensemble. Three simple circulation indices—based on mean sea level pressure, 500-hPa vertical velocity, and 200-hPa velocity potential—are computed for each member of the two ensembles. The study uses the output of the CMIP5 idealized transient climate simulations with 1% yr^{-1} CO_2 increase from preindustrial level, and investigates the detected circulation response until the moment of CO_2 doubling (70 yr). Depending on the indexing method, it is found that 50%–93% of the MPI-ESM-LR and 54%–75% of the CMIP5 ensemble members project significant negative trends in the circulation's intensity. This large spread in the ensembles reduces the confidence that a weakening circulation is a robust feature of climate change. Furthermore, the similar magnitude of the spread in both ensembles shows that the Walker circulation response is strongly influenced by natural variability, even over a 70-yr period.

1. Introduction

The effects of the increased anthropogenic greenhouse gas emissions over the last two centuries have been investigated mostly from the point of view of the thermodynamical response of the climate system (Shepherd 2014). This allows us to build an understanding of the expected changes in the global patterns of climate variables, but still leaves a wide margin for uncertainty in regional climate changes. The regional response to anthropogenic forcing is highly dependent on atmospheric circulation (global and regional), but global circulation models (GCMs) have yet to provide a high confidence level in simulating and projecting these circulation changes (Shepherd 2014).

Under these considerations, this work investigates the variation in a warmer climate of one of the large-scale overturning circulations, namely, the Pacific Walker circulation. Recent studies (Held and Soden 2006; Vecchi and Soden 2007; Chadwick et al. 2013; Bony et al. 2013) suggest that tropical overturning circulations are, in general, weakening as a response to increased CO_2 forcing, which is also expected to hold for the Walker circulation (Power and Kociuba 2011a,b; Ma and Xie 2013). Conversely, the observations of the past two decades have shown a strengthening of the Pacific Walker cell (England et al. 2014). Kociuba and Power (2015) found this variation to be difficult to simulate in phase 5 of the Coupled Model Intercomparison Project (CMIP5) state-of-the-art GCMs in coupled climate experiments with prescribed natural and anthropogenic forcings from observations in the last 150 years (the CMIP5 historical experiment; Taylor et al. 2012). However, another study, based on noncoupled climate experiments with prescribed sea surface temperatures from observations (the AMIP experiment; Taylor et al. 2012; Ma and Zhou 2016), suggests that there is reasonably good performance in the simulation of the strengthened circulation by the CMIP5 models. We can conclude that we still do not fully understand the drivers of the Walker circulation and its internal variability. Therefore, there is a high degree of uncertainty in simulating the behavior of the Walker circulation arising

Corresponding author: Elina Plesca, elina.plesca@uni-hamburg.de

DOI: 10.1175/JCLI-D-17-0151.1

from this lack of knowledge and from the model performance in representing the impact of external forcing of the factors determining the changes in the circulation.

Taking into account this uncertainty, here we look into the variation of the Walker circulation in an idealized transient climate simulation, which describes a climate state closer to present conditions. In particular, we investigate the robustness of the weakening of the circulation in a CMIP5 transient climate experiment, namely the benchmark 1% yr^{-1} increase in CO_2 concentration (from preindustrial levels to quadrupling of concentration), referred to henceforth by its CMIP5 label of 1pctCO2. The initial conditions of the experiment, as well as the differences between GCMs' physics and parameterization schemes, are expected to cause the intermodel spread and subsequent uncertainty in the simulation of the dynamical changes over the Pacific. The novelty of this study is that we consider not only these two factors, but also the method used to quantify the intensity of the Walker circulation. In other words, we inspect the detected circulation response from three distinct perspectives: the internal variability, the GCM configuration, and the indexing method.

The influence of internal variability on the detection of a weakening Walker circulation will be deduced from the output of a 68-member ensemble of the MPI-ESM-LR model. The members of this ensemble differ only in initial conditions: the initial climate state for each member is derived from distinct time windows of the control run of this model.

The second ensemble used in this work comprises 28 CMIP5 GCMs (one realization each). The initial conditions for the 1pctCO2 output differ as in the case of the MPI ensemble, but this ensemble also includes a signal of the differences between the model configurations and parameterization schemes. As mentioned in Shepherd (2014) and Bony et al. (2013), the simulation of the dynamical aspect of climate change is quite dependent on the interaction between the simulations of large-scale systems and small-scale processes. Under this consideration, we analyze the output of this ensemble from the aspect of the nonlinear effects caused by the model configuration in addition to the effect of natural variability.

The third investigated factor is the indexing method applied to quantify the intensity of the Pacific Walker cell. The need for this factor arises from the fact that most studies rely on a single indexing method to describe the intensity of the circulation (e.g., Wang 2002; Tanaka et al. 2004; Vecchi et al. 2006; Bayr et al. 2014). Consequently, additional spread in the projected responses of the Pacific Walker cell may be caused by the internal variability and the response of the index's base parameter to increased CO_2 forcing [see chapter 12 in IPCC (2013)]. Our analysis provides a comparative view of three simple, widely used indices and the circulation response differences that arise from their application.

The main driver of the Pacific Walker cell is the temperature gradient between the eastern and western Pacific. This gradient is accompanied by a pressure gradient across the Pacific. Under these considerations, perhaps the most intuitive index for the Pacific Walker circulation is based on the mean sea level pressure (MSLP) difference between the eastern and western equatorial Pacific (Vecchi et al. 2006). This index will be referred to as the MSLP index. The other two indices investigated here reflect the dynamics of the cell. The ω_{500} index is derived from the 500-hPa vertical velocity anomaly difference between the eastern and western equatorial Pacific (Wang 2002). The third index was introduced by Tanaka et al. (2004) as a characteristic of the circulation in the upper troposphere, is based on the annual deviation from the zonal mean of the 200-hPa velocity potential, and will be referred to as the χ_{200} index (see section 2).

As mentioned above, the response of the index's base parameter to increasing forcing may induce additional uncertainty in the Walker circulation projection. The three indices investigated in this paper are based on parameters highly sensitive to regional cloud and precipitation pattern changes (e.g., surface pressure) and thus are subject to the uncertainty of cloud and precipitation representation in GCMs (Held and Soden 2006; Power and Kociuba 2011a,b; Bony et al. 2013).

We acknowledge that there are other indices quantifying the circulation intensity from anomalies extending over several atmospheric layers (e.g., based on the zonal mass streamfunction; see Yu and Zwiers 2010). Nonetheless, we chose these three simple, all quasi-surface indices, as their derivation is comparable and each of them reflects the circulation at different levels in the atmosphere. This will further allow us to look into the sensitivity of the Walker circulation response to the representation of various processes within the Walker cell.

The time series of the three indices are derived for the two ensembles mentioned above. Following this derivation, index-based differences between trends in the Pacific Walker cell intensity are analyzed, as are the correlations between the indices. Models will be grouped depending on their Walker circulation response in an attempt to reveal possible sources of uncertainties and inconsistencies between GCMs. We start with the premise that differences among models may also be detected in the patterns of parameters whose response to climate change is robust among the CMIP5

TABLE 1. Details of CMIP5 ensemble members. (Expansions of acronyms are available online at http://www.ametsoc.org/PubsAcronymList.)

Model	Horizontal grid points (lat × lon)	Institution
ACCESS1.3	145 × 192	Commonwealth Scientific and Industrial Research Organisation and Bureau of Meteorology, Australia
BCC_CSM1.1	64 × 128	Beijing Climate Center, China Meteorological Administration, China
BCC_CSM1.1-M	160 × 320	
CanESM2	64 × 128	Canadian Centre for Climate Modelling and Analysis, Canada
CCSM4	192 × 288	National Center for Atmospheric Research, United States
CESM1(BGC)	192 × 288	Community Earth System Model contributors, United States
CMCC-CM	240 × 480	Centro Euro-Mediterraneo per I Cambiamenti Climatici, Italy
CNRM-CM5	128 × 256	Centre National de Recherches Météorologiques, Meteo-France, France
CNRM-CM5.2	128 × 256	
CSIRO Mk3.6.0	96 × 192	Commonwealth Scientific and Industrial Research Organization and Queensland Climate Change Centre of Excellence, Australia
FGOALS-g2	60 × 128	Institute of Atmospheric Physics, Chinese Academy of Sciences, and Tsinghua University, China
FGOALS-s2	108 × 128	
GFDL CM3	90 × 144	NOAA/Geophysical Fluid Dynamics Laboratory, United States
GFDL-ESM2G	90 × 144	
GFDL-ESM2M	90 × 144	
GISS-E2-H	90 × 144	NASA Goddard Institute for Space Studies, United States
HadGEM2-ES	145 × 192	Met Office Hadley Centre, United Kingdom
INM-CM4.0	120 × 180	Institute of Numerical Mathematics, Russia
IPSL-CM5A-LR	96 × 96	Institute Pierre-Simon Laplace, France
IPSL-CM5A-MR	143 × 144	
IPSL-CM5B-LR	96 × 96	
MIROC-ESM	64 × 128	Japan Agency for Marine-Earth Science and Technology, Atmosphere and Ocean Research Institute (The University of Tokyo), and National Institute for Environmental Studies, Japan
MIROC5	128 × 256	
MPI-ESM-LR	96 × 192	Max Planck Institute for Meteorology, Germany
MPI-ESM-MR	96 × 192	
MRI-CGCM3	160 × 360	Meteorological Research Institute, Japan
NorESM1-M	96 × 144	Norwegian Climate Centre, Norway
NorESM1-ME	96 × 144	

models, such as global mean surface temperature increase and mean outgoing longwave radiation decrease over the tropical Pacific [see chapter 12 in IPCC (2013)].

This paper is structured as follows: section 2 describes the datasets and gives a more elaborate definition of the Walker circulation indices, section 3 contains results and discussion, and section 4 draws conclusions and points out some considerations on further application of the findings.

2. Data and methods

a. Data

To identify patterns of the Walker circulation changes in a transient climate, we focus this study on the CMIP5 idealized experiment with 1% yr^{-1} increase in CO_2 concentration relative to preindustrial levels, run until quadrupling of concentration, but we also use output of the preindustrial control experiment, which is henceforth referred to as piControl (Taylor et al. 2012). Monthly mean output of two ensembles are used. The first ensemble consists of 68 members resulting from the MPI-ESM-LR model with slightly perturbed initial climate state at each run, derived from different time windows in piControl (referred to onward as the MPI ensemble). The second ensemble comprises monthly output for the CMIP5 experiments from 28 GCMs listed in Table 1. (referred to as the CMIP5 ensemble). For every CMIP5 GCM, one realization of the model was considered, namely the r1i1p1 realization (Taylor et al. 2012). The version of the MPI-ESM-LR model applied for obtaining the MPI ensemble is different from the model version in the CMIP5 ensemble; therefore, differences in values and responses are to be expected.

Although the 1pctCO2 experiment is idealized, we also use ERA-Interim monthly means for the 1979–2014 period to look into the current state of the transient climate. We consider these values as reference values for assessing whether the Walker circulation is realistically simulated in the idealized transient climate experiment.

b. Methods

Three indices for the intensity of the Pacific Walker cell are compared in this work. The MSLP index relates to the main driver of the Walker circulation: the temperature gradient across the tropical Pacific, which may also be derived from the pressure gradient. This index is computed following Vecchi et al. (2006) and is equal to the difference between the MSLP anomaly (deviation from the mean MSLP for the experiment time range, 140 years, that corresponds to the moment of CO_2 quadrupling) averaged over the eastern equatorial Pacific (5°S–5°N, 160°–80°W) and the western equatorial Pacific (5°S–5°N, 80°–160°E).

The second index, the ω_{500} index, looks into the vertical motion in the ascending and subsiding branches of the Pacific Walker cell. It is derived from the mean 500-hPa vertical velocity anomaly (deviation from the mean 500-hPa vertical velocity for the experiment time range, 140 years, that corresponds to the moment of CO_2 quadrupling) difference between the eastern equatorial Pacific (5°S–5°N, 160°–120°W) and the western equatorial Pacific (5°S–5°N, 120°–160°E), as described in Wang (2002).

The third method of indexing the Walker circulation is based on the decomposition of the 200-hPa velocity potential field in three orthogonal spatial patterns—zonal, time mean eddy, and transient eddy components—each describing the Hadley, Walker, and monsoon circulations, respectively (Tanaka et al. 2004). Following this method, the χ_{200} index of the Walker circulation is defined as the maximum value over the western Pacific in the 12-month running mean field of the deviation from the zonal mean for the 200-hPa velocity potential. The definition of the index also provides an indication of the approximate geographical position for the ascending branch of the cell in addition to the intensity quantification.

Note that the reference boxes for the MSLP index and ω_{500} index differ, and the reference grid point for the χ_{200} index varies between time steps. Additionally, because the seasonality of the χ_{200} index is removed by applying a 12-month running mean, we apply the same averaging method to the time series of the MSLP index and the ω_{500} index to ensure equivalent comparison.

To investigate the relationship between the change in the Walker circulation and the mean surface temperature change, we look into transient climate response (TCR), which was first introduced by Cubasch et al. (2001) as the mean global surface temperature change ΔT by the time of CO_2 doubling under a scenario equivalent to the 1pctCO2 experiment. TCR is usually applied to characterize the mean climate state in a transient climate, being different from equilibrium climate sensitivity (ECS), which reflects the changes of the system after equilibrium is reached (Gregory and Forster 2008). TCR is most commonly calculated as the mean global ΔT for years 61–80 of the 1pctCO2 output, after the control run mean global temperature is removed. Gregory and Forster (2008) introduce a new method for TCR calculation from the radiative forcing at the time of CO_2 doubling and the climate resistance parameter, thus removing the need to use the control runs of the models. By deriving TCR with both methods, as well as with linear regression of the time series, we find that the difference between TCR derived with the Gregory and Forster (2008) method and with linear regression is on the order of 10^{-3} K for the MPI ensemble and on the order of 10^{-2} K for the CMIP5 ensemble. The difference between these methods and the first method is on the order of 10^{-1} K for both ensembles. Considering that the method introduced by Gregory and Forster (2008) accounts for the gradual increase in forcing and for the climate system resistance to the changes induced by this forcing, we will consider this as reference method for the calculation of TCR.

However, the comparison of global TCR to Walker circulation changes introduces additional uncertainty to the conclusion, as global TCR is also subject to variations in the subtropical and polar regions' circulation. Consequently, in the framework of this paper, we define the tropical Pacific TCR (TCR_{TP}) equal to ΔT in the region within the box 30°S–30°N, 80°E–80°W by the time of CO_2 doubling. This box covers all regions used in the derivation of the Walker circulation indices. At the same time, TCR_{TP} cannot be derived directly by using the Gregory and Forster (2008) method, since that method relies on global averages. To simplify the calculation of TCR_{TP}, we use the linear regression method. This is justified by the small difference between this method and the Gregory and Forster (2008) method.

3. Results and discussion

This section presents the analysis of the time series for the Pacific Walker circulation indices. It discusses the results for the MPI ensemble (section 3a) and the CMIP5 ensemble (section 3b) and examines the differences between ensemble members (section 3c).

a. MPI-ESM-LR ensemble

As stated above, the intent of using the MPI ensemble is to study the impact of natural variability on the Walker circulation trend. Averaging over the 68 members of the MPI ensemble, the mean values over the time series of the MSLP, ω_{500}, and χ_{200} indices are -0.038 ± 0.398 Pa,

TABLE 2. Statistical results for the MPI and CMIP5 ensembles. The Pearson correlation coefficient between x and y is given by corr(x, y).

	MPI ensemble		CMIP5 ensemble		
	Mean	σ	Mean	σ	ERA-Interim
MSLP index[a] (Pa)	−0.038 ± 0.398	75.542 ± 6.787	0.129 ± 0.446	71.545 ± 21.732	4.099 ± 83.576
ω_{500} index[a] (10^{-3} Pa s^{-1})	0.019 ± 0.049	9.574 ± 0.945	−0.015 ± 0.087	13.027 ± 4.922	0.299 ± 18.853
χ_{200} index[a] (10^5 m^2 s^{-1})	134.213 ± 0.869	10.019 ± 0.739	119.241 ± 25.425	11.041 ± 3.506	108.764 ± 10.012
All months in the Walker circulation index time series					
Corr(MSLP index, ω_{500} index)	−0.435 ± 0.136		0.203 ± 0.548		0.753
Corr(MSLP index, χ_{200} index)	0.398 ± 0.062		0.337 ± 0.262		0.427
Corr(ω_{500} index, χ_{200} index)	0.256 ± 0.084		0.307 ± 0.243		0.613
Months in the Walker circulation index time series with extreme circulation intensity					
Corr(MSLP index, ω_{500} index)$_{\text{extreme}}$	−0.214 ± 0.359		0.380 ± 0.664		0.884
Corr(MSLP index, χ_{200} index)$_{\text{extreme}}$	0.574 ± 0.213		0.535 ± 0.385		−0.400
Corr(ω_{500} index, χ_{200} index)$_{\text{extreme}}$	0.299 ± 0.221		0.367 ± 0.422		−0.110
Variations of parameters until CO_2 doubling					
MSLP index trend (Pa decade^{-1})	−1.553 ± 0.388		−4.477 ± 4.328		—
ω_{500} index trend (10^{-3} Pa s^{-1} decade^{-1})	−0.725 ± 0.753		−0.516 ± 1.101		—
χ_{200} index trend (10^5 m^2 s^{-1} decade^{-1})	−1.113 ± 0.592		−0.395 ± 0.955		—
TCR_{TP} (K)	1.547 ± 0.079		1.592 ± 0.302		—

[a] For each index and each ensemble member, we calculate the mean of its time series (140-yr period, which corresponds to CO_2 quadrupling), and the standard deviation of its detrended time series. The table presents the averages of these values and their variance within the corresponding ensemble.

$0.019 \pm 0.049 \times 10^{-3}$ Pa s^{-1}, and $134.213 \pm 0.869 \times 10^5$ m^2 s^{-1}, respectively (Table 2). These mean values differ from the ERA-Interim mean values, but the high variance within the reanalysis still places them within one standard deviation (1σ) from the mean for the first two indices and around 2σ from the mean for the χ_{200} index. The ERA-Interim mean value shows a stronger circulation in comparison to the MPI ensemble mean based on the MSLP and ω_{500} indices, but slower based on the χ_{200} index. Here we acknowledge that these differences arise from 1) the setup of the CMIP5 1pctCO2 experiment as an idealized climate experiment; 2) the distinct configuration of the model on which the ERA-Interim reanalysis dataset is based (compared to the configuration of the MPI-ESM-LR model); 3) the different time extent for the averaging, which takes into account more internal variability modes for the CMIP5 experiment than for ERA-Interim; and 4) the fact that ERA-Interim relies on a period which was shown to have a stronger Walker circulation (England et al. 2014).

We also acknowledge that the definitions of the MSLP and ω_{500} indices suggest the time mean of these indices should tend to zero. However, the choice of the spatial boxes used to derive the mean anomalies in the convection and subsidence branches of the Walker cell can explain the nonnull values. The western boxes used in the derivation of the indices include considerable landmass. Therefore, in comparison with the eastern box, the western anomalies will also arise from the effect of land–sea contrast. Another reason for a nonnull mean value could be related to the difference between the convection and subsidence areas: the former is more aggregated than the latter, and the eastern box may not contain the entire subsidence area related to the Pacific Walker cell. Despite this feature of the index definition and the differences between the 1pctCO2 experiment and the reanalysis mean values, we consider the MPI ensemble values realistic and comparable with values obtained in previous studies for time series of observation and/or reanalysis datasets (Wang 2002; Tanaka et al. 2004; Vecchi et al. 2006).

As mentioned above, each of these indices describes a distinct feature of the Pacific Walker cell, is subject to thermodynamical and circulation processes at different levels in the atmosphere, and is built on different basis variables and geographical regions. Table 2 gives time series statistics, including trend and correlation coefficient statistics, for the reanalysis, both ensembles and the investigated indices. The reanalysis dataset reveals a fairly good correlation between the MSLP and ω_{500} indices (0.753), as well as between the ω_{500} and χ_{200} indices (0.613), but this correlation is quite low between the MSLP and χ_{200} indices (0.427). We also consider the relation between El Niño–Southern Oscillation and the Walker circulation–El-Niño events related to weakened circulation. La Niña events are consistent with a strengthened Pacific Walker cell, but the index variance during these periods is significantly smaller than during El Niño periods (Tanaka et al. 2004). We therefore correlate the months with circulation intensity outside

1σ from the mean of the time series for all three indices (hereafter named extreme cases). It is found that all the identified extreme cases relate to a strongly weakened circulation. While the correlation coefficient between the MSLP and ω_{500} indices becomes larger, it becomes negative and considerably smaller for the correlations between these two indices and the χ_{200} index. This results from the latter reaching a minimum of intensity 4–5 months later than the first two indices (not shown), suggesting a slower response of the upper troposphere to a weaker circulation. Considering the differences between indices' definitions and the medium-to-high correlations between the time series, the correlation results for the ERA-Interim time series are deemed realistic.

Interestingly, the correlation within the MPI ensemble is inconsistent with the reanalysis, showing not only smaller correlation coefficients but also negative correlation between the MSLP and ω_{500} indices (Table 2). The latter may be attributed to various reasons, such as the definition of the indices, discrepancies between the surface pressure and vertical velocity response to circulation intensity change, and the physical approximations and parameterization schemes of the MPI-ESM-LR. A thorough analysis of this feature is beyond the scope of this work, but may serve as a good test case for the performance of a GCM. With the abovementioned negative correlation in mind, we find that while looking into the extreme cases for this ensemble, the MSLP and ω_{500} indices are practically uncorrelated. While the mean ensemble correlation between the χ_{200} index and the other two indices increases for the extreme cases, its variance also becomes larger. The reasons for such values stated for the ERA-Interim dataset apply here as well, along with the fact that for the MPI ensemble the time lag between the minima in the χ_{200} index and the other two indices' time series is around 7–8 months. Davis and Birner (2016) also noticed this interesting fact that the correlation between different indexing methods is stronger in reanalysis than in GCM simulations, although their observations were for the Hadley circulation and the width of the tropical belt instead of the Walker circulation. The reason for this apparently general behavior is unclear; it may be caused by insufficient precision in the GCM simulation of the circulation, but also may simply be due to the much higher resolution of reanalysis.

The trends in the intensity of the Pacific Walker cell were derived by applying time linear regression to the three indices' time series. Index-wise, the mean trends over the MPI ensemble until the moment of CO_2 doubling (70 yr) and quadrupling (140 yr) are shown in Table 2. On average, independent of the chosen index, the Walker circulation has slowed down at the time of CO_2 doubling. Compared to the ensemble mean standard deviation of the indices, the trend suggests a decrease in the intensity of the cell by 2.1%, 7.6%, and 11.1% σ decade^{-1} for the MSLP, ω_{500}, and χ_{200} indices, respectively (Table 2). But the percentage of members simulating a weakening circulation varies among indices. Here we consider as significant the trends with $\geq$80% confidence level, and we observe the following for each of the indices' time series:

1) MSLP index, 49 out of 68 ensemble members show significant trends, of which 34 are negative (suggesting a weakening Walker circulation by the moment of CO_2 doubling);
2) ω_{500} index, 59 out of 68 ensemble members show significant trends, of which 54 are negative; and
3) χ_{200} index, 63 out of 68 ensemble members show significant trends, of which all are negative.

These results suggest a degree of sensitivity of the circulation projection to surface processes, which induces additional variability for the indices. The lower troposphere branch of the Pacific Walker cell is highly dependent on the thermodynamics and atmospheric circulation within the boundary layer and is also influenced by the atmosphere–ocean coupling. The MSLP index, which is characterizing the intensity of this section of the cell, shows the lowest percentage of significant trends (72%) and the lowest percentage of ensemble members projecting a weakening circulation by the doubling of CO_2 (50% of all ensemble members and 69% of the ensemble members with significant trends). In the case of the ω_{500} index, which describes the change in the ascending branch of the cell and is less sensitive to surface processes, there are more ensemble members that have a significant trend (87%). Also, the probability of a weakening circulation is higher if this index is considered, as 79% of ensemble members project the weakening (92% of the ensemble members with significant trends). The upper troposphere is significantly more stable than its lower and middle parts and exhibits less variability on monthly scales. As a result, for the χ_{200} index time series we find significant trends in 93% of the ensemble members, all of which suggest a weakening circulation. To conclude, the detection of trends in the intensity of the Walker circulation is affected by the sensitivity of the base parameter to surface processes, including the atmosphere–ocean coupling in the lower troposphere. Some of the variability may also be a result of the index definition; whereas Tanaka et al. (2004) separate the Walker circulation from the Hadley and monsoon circulations, the other two indices might still contain significant variability modes originating from these circulations.

TABLE 3. Ensemble correlation between the change in Walker circulation on one side and TCR_{TP} on the other side (selected runs/GCMs refer to the runs/GCMs that show a significant trend in the Walker circulation intensity until CO_2 doubling).

	MPI ensemble		CMIP5 ensemble	
	All runs	Selected runs	All GCMs	Selected GCMs
MSLP index	−0.774	−0.826	−0.338	−0.323
ω_{500} index	0.152	0.150	0.047	−0.094
χ_{200} index	−0.534	−0.546	−0.370	−0.454

The most robust feature in the response of the climate system to increased CO_2 forcing is mean surface temperature rise. Previous studies show that the tropical overturning circulation is slower in a warmer climate (Held and Soden 2006; Vecchi and Soden 2007; Chadwick et al. 2013; Bony et al. 2013). In this regard, we looked into the relationship between the change in the intensity of the Walker circulation and the change in mean surface temperature in the tropical Pacific region. Considering the above, a negative correlation should be expected. The MPI ensemble tropical mean ΔT by CO_2 doubling, TCR_{TP}, is 1.547 K and has a low variance, as shown in Table 2. The trends detected in the Walker circulation indices have considerably higher variance (Table 2); therefore, high correlation between TCR_{TP} and the circulation changes across the ensemble is less probable, as seen in Table 3. TCR_{TP} has the highest absolute correlation coefficient value with the MSLP index trend, which is expected, considering the dependence of the MSLP index on surface temperature changes. The ω_{500} index trend shows the highest variance within the MPI ensemble (Table 2), which may in turn explain the detected insignificant correlation coefficients. If only runs with significant detected trends are considered, the correlation between the changes in the circulation and in the surface temperature slightly improves for the MSLP and χ_{200} indices, but this does not hold for the ω_{500} index.

As mentioned in the definition of the χ_{200} index, this method also provides an indication of the location of the ascending branch of the Walker cell. By analyzing the time series of the coordinates for the maximum value of χ_{200}, we find that 90% of the MPI ensemble members suggest an eastward shift of the ascending branch, which is consistent with previous findings (Bayr et al. 2014).

In conclusion of this subsection, based on the MPI ensemble, we note that internal variability alone causes a significant spread in the response of the Pacific Walker circulation to increasing CO_2 forcing. The robustness of a weakening circulation is diminished by the differences between the trends detected in the time series of the three indices and by the relatively low correlation between these indices. In general, the χ_{200} index provides the highest confidence in the detected trend and in the sign of the circulation's intensity change, leading us to rely on it for further studies. At the same time, this index is a proxy for the upper-tropospheric divergence of flow resulting from the circulation, being less representative for the ascending branch or the lower tropospheric flow within the Pacific Walker cell. Consequently, in future studies, the choice of index should depend on the scope and region of study.

b. *CMIP5 ensemble*

In this subsection we look into another kind of ensemble, the CMIP5 model ensemble. Here, each ensemble member has different model physics. Initial conditions also differ, but the main source of differences is generally seen in the GCM configuration. The 28 members of the CMIP5 ensemble render time averaged MSLP and ω_{500} indices slightly different in value and variance from the case of the MPI ensemble. As in the case of the MPI ensemble, these values differ from the ERA-Interim resulting averages (Table 2). The χ_{200} index shows a CMIP5 ensemble mean value that is smaller than the MPI ensemble value but closer to the ERA-Interim to a degree of one standard deviation. The considerations stated in the previous subsection about the differences between datasets are also valid for this ensemble. Also, these differences and the higher variance come from the nonlinear effects of the numerical approximations and parameterization schemes characteristic to each GCM. Under these considerations, we assume that the simulations capture the Walker circulation reasonably well.

The correlation between indices is low and significantly more varying within this ensemble compared to both the MPI ensemble and the reanalysis values. The differences between the physics of the CMIP5 GCMs make it impossible to conclude about the correlations between the indices on ensemble level (both for the entire time series and for the extreme cases), even though for specific models some coefficients are large. For example, the correlation between the MSLP and χ_{200} indices for MIROC-ESM is 0.855, but it is quite low between the ω_{500} and χ_{200} indices (0.322) and between the MSLP and ω_{500} indices (0.179). The large variance of the correlation coefficients suggests a different response

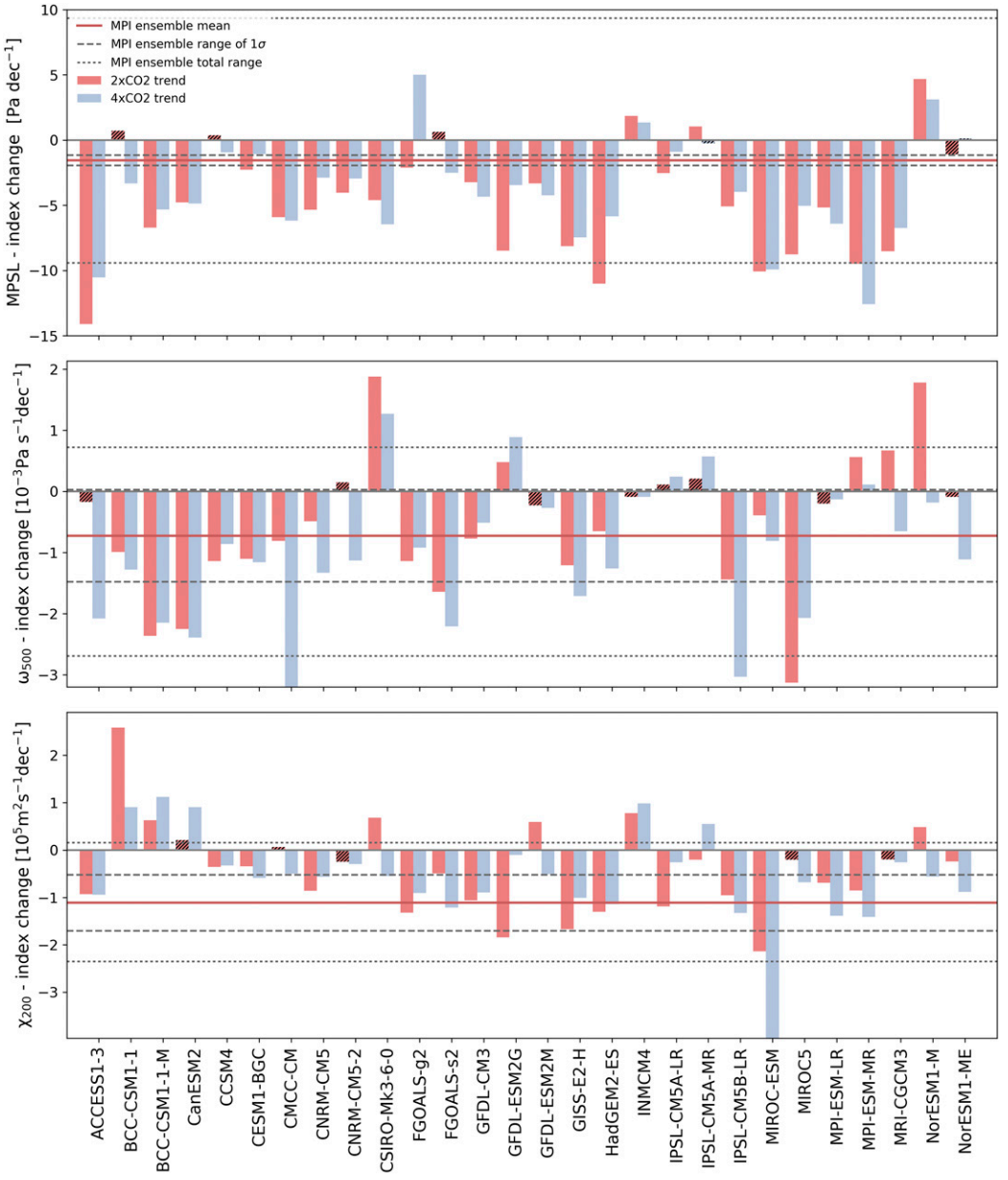

FIG. 1. Pacific Walker cell intensity trends detected for the CMIP5 ensemble 1pctCO2 experiment output. Trends detected until CO_2 doubling are bars shaded red, and until CO_2 quadrupling are bars shaded blue. Hatched bars denote trends with confidence level below 80%. The red solid line represents the MPI ensemble mean trend, the dashed lines represent the range of 1σ variance, and the dotted lines represent the total spread of the MPI ensemble.

of the circulation at different vertical levels, pointing to a probable degree of discontinuity in the vertical in some GCMs and/or a need to adjust the indices to the particular GCM.

As seen in Table 2, the mean CMIP5 ensemble trend in the Pacific Walker cell is negative, regardless of the chosen index. On average, during the period until CO_2 doubling, the circulation is slowing down by 6.3%, 4.0%, and 3.6% σ decade^{-1} for the MSLP, ω_{500}, and χ_{200} indices, respectively (Table 2). The values of the mean trend differ significantly from the MPI ensemble, and their variance is considerably larger. Figure 1 depicts the Walker circulation 70-yr trends (until CO_2 doubling) and 140-yr trends (until CO_2 quadrupling) over the CMIP5 ensemble. Independent of the index, at least 70% of the ensemble members show significant trends,

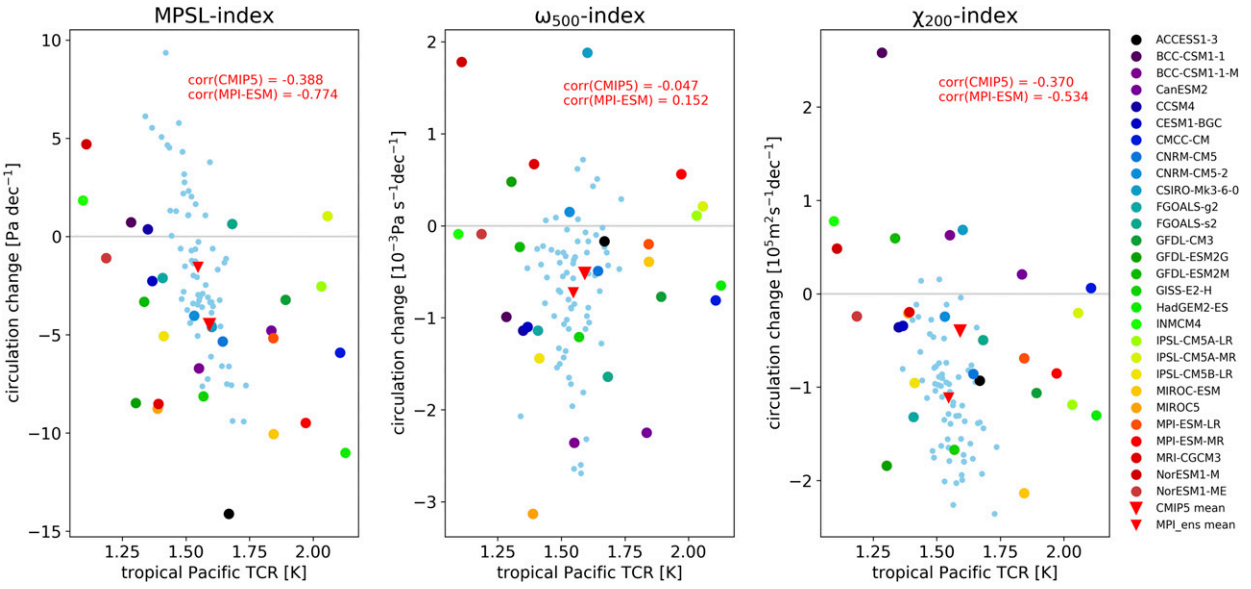

FIG. 2. Pacific Walker cell intensity trend until CO_2 doubling compared to the TCR_{TP} in the CMIP5 and MPI ensembles' output of the 1pctCO2 experiment (the values corresponding to the MPI ensemble are denoted by light blue dots with smaller diameters). The correlation coefficient between the two sets is given for each ensemble separately.

as defined in the previous section (24 out of 28 for the MSLP index; 20 out of 28 for the ω_{500} index; and 23 out of 28 for the χ_{200} index). A weakening Pacific Walker cell is simulated by the following:

1) 21 out of 24 members with significant trend in the MSLP index time series;
2) 15 out of 20 members with significant trend in the ω_{500} index time series; and
3) 17 out of 23 members with significant trend in the χ_{200} index time series.

Regarding the ability to detect significant trends, the CMIP5 ensemble shows less sensitivity to surface processes than the MPI ensemble does. However, the number of members and the distinct configuration of the GCMs caution against drawing conclusions from this difference in sensitivity.

Nonetheless, as in the case of the MPI ensemble, the same model may suggest a different sign for the change in the circulation intensity depending on the chosen index (Fig. 1). As the 1pctCO2 experimental setup in CMIP5 allows investigation of changes until quadrupling of CO_2, we note in Fig. 1 that some models reveal significantly different trends in the circulation from the start of the experiment until doubling of CO_2 (70-yr period) than until quadrupling (140-yr period)—for example, BCC_CSM1.1, FGOALS-s2, and MIROC-ESM. This feature holds also for the trends detected from the moment of CO_2 doubling until that of quadrupling (not shown). This leads to the conclusion that the intensity change is not entirely due to the increasing forcing but is also partly due to the internal variability of the Pacific Walker circulation and its driving factors.

To assess the importance of increased forcing for the circulation change, we look again to the TCR_{TP} as a robust indicator of the response of the climate system to higher CO_2 concentration. Figure 2 depicts the change in circulation as a function of TCR_{TP} for each member of both investigated ensembles. There is one panel for each circulation index. As clearly visible, the CMIP5 ensemble mean TCR_{TP}, 1.592 K (Table 2), does not differ significantly from the MPI ensemble mean TCR_{TP}, but the GCMs' distinct configurations lead to a much higher variance ($\sigma = 0.302$ K). These large variances of TCR_{TP} and of the Walker circulation indices affect the detection of correlation between these parameters, giving significantly different values compared to the MPI ensemble (Table 3). Limiting the correlation only to the GCMs showing significant trends does not improve the correlation either.

In summary, it is interesting to note that, although somewhat larger, the spread in the detected Walker circulation intensity change found in the CMIP5 ensemble is of comparable magnitude to the spread found in the MPI ensemble.

c. *Ensemble members comparison*

Judging from Fig. 2, it is apparently sufficient to use one GCM ensemble (in this case, the MPI ensemble) to obtain the variance of the Walker circulation trends

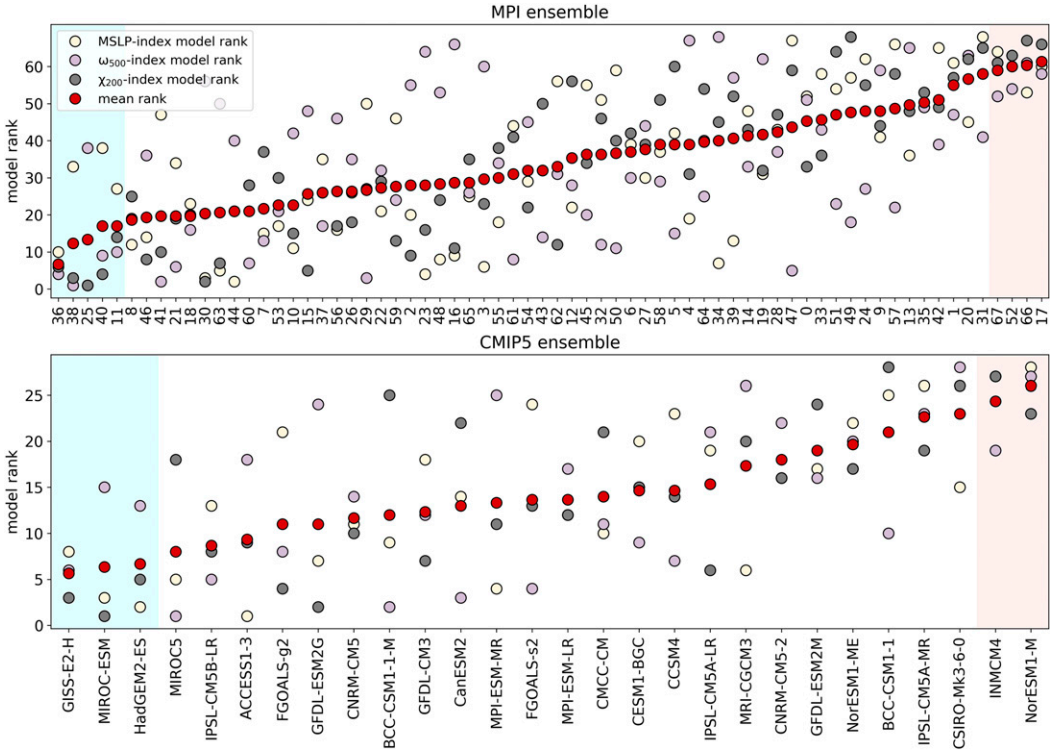

FIG. 3. (top) MPI and (bottom) CMIP5 ensemble members' index-based ranking (in ascending order), according to the projected trend in the intensity of the Pacific Walker cell until CO_2 doubling within the 1pctCO2 experiment (MPI-ESM-LR runs and CMIP5 GCMs are ordered according to their mean rank). The blue shading denotes the LRMs (projecting on average the strongest weakening of the Walker circulation), and the red shading denotes the HRMs (projecting on average the smallest weakening of the Walker circulation or its strengthening).

under increased CO_2 forcing. In other words, it appears at first sight as if natural variability alone could account for the observed intermodel spread in Walker circulation response. We investigated this point further, looking for differences between GCM representation of the Walker circulation in a control unforced climate experiment and for qualitative differences between Walker circulation response spread in the two different ensembles.

Before looking into these differences, we rank the MPI and CMIP5 ensembles' members in ascending order by each Walker circulation index time series trend. Figure 3 shows the order of the ensemble members arranged according to their mean rank across the three indices. Again, Fig. 3 draws attention to the differences between the trends detected in the time series of the three indices—unless by mean rank, the low correlation between index rankings makes it difficult to indicate which model shows the largest weakening or strengthening of the Walker circulation. Furthermore, we use the 5th and 95th percentile of the mean rank rank_m across each ensemble to distinguish two groups of MPI-ESM-LR runs and CMIP5 GCMs (Fig. 3):

1) low-ranking ensemble members (LRMs) or members that project the strongest weakening of the Walker circulation: MPI-ESM-LR runs with $\text{rank}_m \leq 17$ (MPI ensemble 5th percentile) and GCMs with $\text{rank}_m \leq 10$ (CMIP5 ensemble 5th percentile) and
2) high-ranking ensemble members (HRMs) or members that project the smallest weakening of the Walker circulation or even its strengthening: model runs with $\text{rank}_m \geq 58$ (MPI ensemble 95th percentile) and GCMs with $\text{rank}_m \geq 23$ (CMIP5 ensemble 95th percentile).

To investigate the simulation of the Walker circulation by the CMIP5 ensemble members, we look into the background naturally forced CMIP5 experiment, namely piControl. A time mean for this control run of the meridional cross section over the equatorial Pacific (between 10°N and 10°S) of the vertical velocity field, hereinafter ω_X, can be used to give an indication of the characteristics of the Pacific Walker cell simulation in the respective GCM and the locations of the corresponding ascending and subsiding branches. Figure 4a

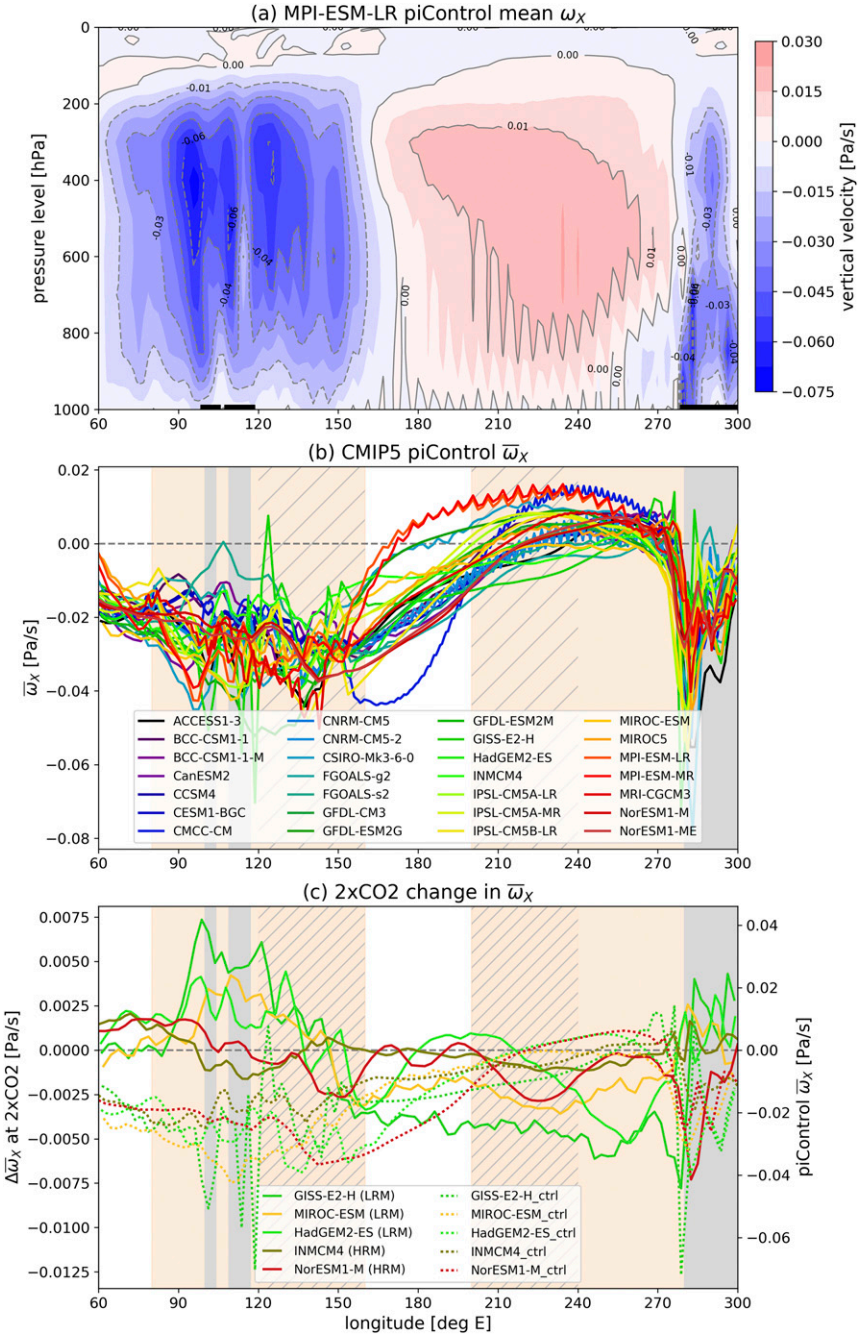

FIG. 4. (a) Meridional cross section of vertical velocity ω_X between 10°N and 10°S, calculated for the mean piControl output of MPI-ESM-LR. (b) CMIP5 ensemble vertically weighted mean $\overline{\omega}_X$ of the meridional cross section presented above. (c) Changes in $\overline{\omega}_X$ at the moment of CO_2 doubling with respect to the control run for the CMIP5 ensemble LRMs (GISS-E2-H, MIROC-ESM, and HadGEM2-ES) and HRMs (INM-CM4.0 and NorESM1-M). Note that the thick black lines at the bottom of (a), as well as the gray stripes in (b) and (c), represent land surface on the equator, corresponding to Sumatra, Borneo, and South America. The beige stripes in (b) and (c) refer to the zonal extent of the boxes used to compute the MSLP index; the hatching refers to the zonal extent of the boxes used to compute the ω_{500} index.

presents such a cross section obtained from the output of the MPI-ESM-LR model, showing a clear differentiation between the convective region in blue shading over the Maritime Continent and the subsidence region in red shading over the central and eastern Pacific. The wavelike features visible in the cross section for this model, as well as MPI-ESM-MR (Fig. 4b), are numerical artifacts resulting from spectral ringing (T. Mauritsen 2017, personal communication). To facilitate the comparison of the Pacific Walker cell representation between the 28 members of the CMIP5 ensemble, we calculate the layer-thickness-weighted vertical mean of ω_X, referred to onward as $\overline{\omega}_X$. The minimum value of $\overline{\omega}_X$ corresponds to the region of strongest convection, and the maximum value to the region with strongest subsidence. As seen in Fig. 4b, the general expected $\overline{\omega}_X$ pattern of the Pacific Walker cell is identifiable in all the models: we find a convective region over the Maritime Continent and a subsidence region over the eastern Pacific. There is also a region of ascending motion starting around 280°E (i.e., 80°W), but this is induced by orography. Nonetheless, there is a large variance of the Walker circulation simulation among the CMIP5 GCMs, especially in the zonal extent and in the average intensity of vertical velocity in these regions. Considering this background experiment variance, we infer that the GCM numerical configuration and its parameterization schemes influence the representation of the Pacific Walker cell and its variation under various forcings. We further investigate the change in $\overline{\omega}_X$ at the moment of CO_2 doubling (averaging over years 60–80 of the 1pctCO2 output) with respect to the piControl mean, in particular for the CMIP5 ensemble LRMs and HRMs. Figure 4c shows this change on the left y axis (solid lines) and the background pattern on the right y axis (dotted lines). There is no clear distinction between the LRMs and HRMs in the piControl experiment. So, apparently, the difference in the response between the LRMs and HRMs is not caused by them having different representation of the Walker circulation to start with, but by other intermodel differences that only become apparent upon forcing. The HRMs show significantly less variance in the change across the equatorial Pacific than the LRMs. Also, the HRM ensemble members suggest a slightly intensified convection in the ascending branch and small change in the subsidence area, which is consistent with a circulation that either has insignificant change or one that strengthens. Conversely, the LRMs clearly show a shift of the convecting branch eastward from the Maritime Continent and a general increase in ascending motion across the Pacific, which is related to a slower circulation. Again, the fact that in the background experiments the low-ranking and the high-ranking ensemble members do not show clear differences suggests that the distinct response found for the Pacific Walker cell is mostly induced by the CO_2 forcing and the response of the climate system elements to this forcing (e.g., clouds, precipitation, surface temperature, atmospheric stratification, atmosphere–ocean heat exchange).

As mentioned in section 3a, increased surface temperature is one of the climate's robust responses to a CO_2 concentration increase and may serve as an intermediate parameter to identify drivers of the circulation response variation. The circulation may be investigated inclusively from the point of view of the related cloudiness and/or outgoing longwave radiation (OLR). The latter is modulated by factors such as clouds, precipitation, aerosols etc. At this moment, because of the low confidence in aerosol–cloud interaction radiative feedback [see chapter 8 in IPCC (2013)], the parameterization of clouds and convection is responsible for most uncertainty in climate models, including in the projection of OLR variation at intra- and interannual time scales. Here we look into the spatial structure of OLR change and surface temperature increase by the doubling of CO_2, as simulated by the ensembles, and investigate the differences among ensemble members in the region of the tropical Pacific. Although the correlation among surface temperature increase, OLR trend, and Walker indices trends is low (not shown), the differences in the regional response of temperature and OLR may be indicative of the origin in Walker circulation change differences among models.

Figure 5 describes for each of the two ensembles the mean ensemble change in OLR with respect to the piControl mean, as well as the change detected in the LRM and HRM groups. Figures 5a,b show that the patterns in the mean control OLR (obtained from averaging over the monthly output of the piControl CMIP5 experiment) are quite similar between the MPI and CMIP5 ensembles, despite the small differences over the central Pacific and eastern Indian Ocean–Australia regions, where the MPI ensemble suggests less cloudiness. Consequently, we deem it reasonable to look into the CO_2-forced OLR changes in both ensembles, aiming to identify the effect of internal variability and of GCM configuration on the mean change. This comparison reveals significant differences between the mean ensemble OLR change: the MPI ensemble shows an increasing cloudiness not only across the central Pacific, but also over the Maritime Continent, whereas the CMIP5 ensemble does not (Figs. 5c,d). Also, the presence and intensification of the southern branch of the intertropical convergence zone (ITCZ) is much more pronounced in the MPI ensemble. The CMIP5 mean OLR change reveals a strong increase of cloudiness

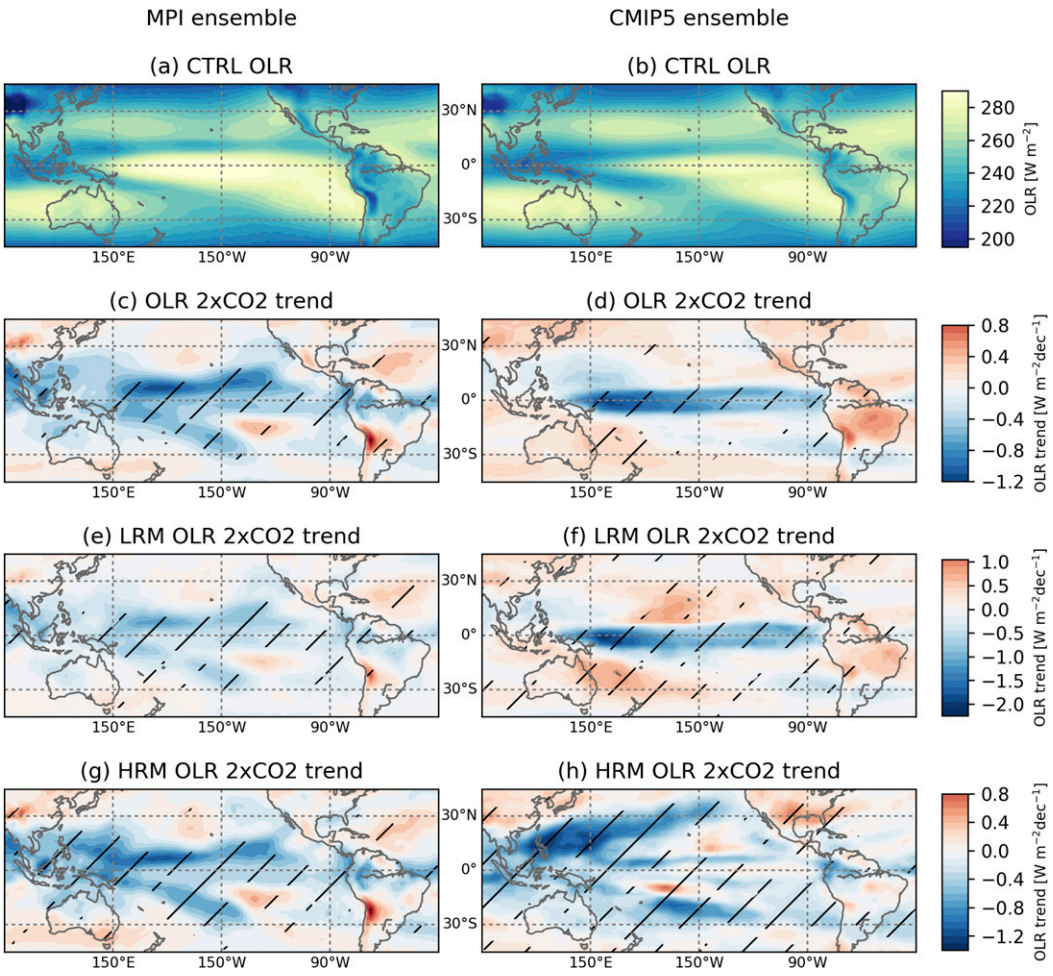

FIG. 5. Ensemble mean OLR in piControl for the (a) MPI and (b) CMIP5 ensembles. (c),(d) As in (a),(b), but for the ensemble mean trend in OLR variation until CO_2 doubling in the 1pctCO2 output. (e),(f) As in (c),(d),but for the mean trend in OLR variation until CO_2 doubling in the 1pctCO2 output, averaged for the LRMs. (g),(h) As in (e),(f), but for the mean OLR trend until CO_2 doubling, averaged for the HRMs. Note that regions with trends having ≥80% confidence level are hatched.

immediately to the east of the Maritime Continent. Therefore, not only do previous studies (Bayr et al. 2014) and the χ_{200} index analysis project this shift of the ascending branch of the cell (75% of the CMIP5 GCMs simulate it; not shown), but it is also confirmed by the OLR change pattern.

We note that the mean MPI ensemble OLR change pattern is preserved in both the LRM and HRM means (Figs. 5e and 5g, respectively) through increasing cloudiness along the equator and the Maritime Continent and the visible southern branch of the ITCZ. The difference between these groups of the MPI ensemble members is mostly in the magnitude, not the sign of the trend. This can be seen in Fig. 6, which shows mean OLR trend differences between HRM and LRM models. Hatching there indicates where the trend changes sign between LRM and HRM models, and Fig. 6a shows that this does not occur over the tropical Pacific for the MPI ensemble. However, it is also visible that compared to the HRM group, the LRM group projects almost no increase in cloudiness over the Maritime Continent; rather, the change is eastward from this region. This is again consistent with an eastward shift of the Walker cell ascending branch in a climate with slower circulation.

Figures 5f and 5h show the mean state of OLR trend for CMIP5 LRM models (GISS-E2-H, MIROC-ESM, and HadGEM2-ES) and HRM models (INM-CM4.0 and NorESM1-M), respectively. Compared to the results from the MPI ensemble, the patterns in the OLR trend differ significantly between the two groups of GCMs. Also, the area showing a different sign in the trends is much larger (Fig. 6b), including parts of the

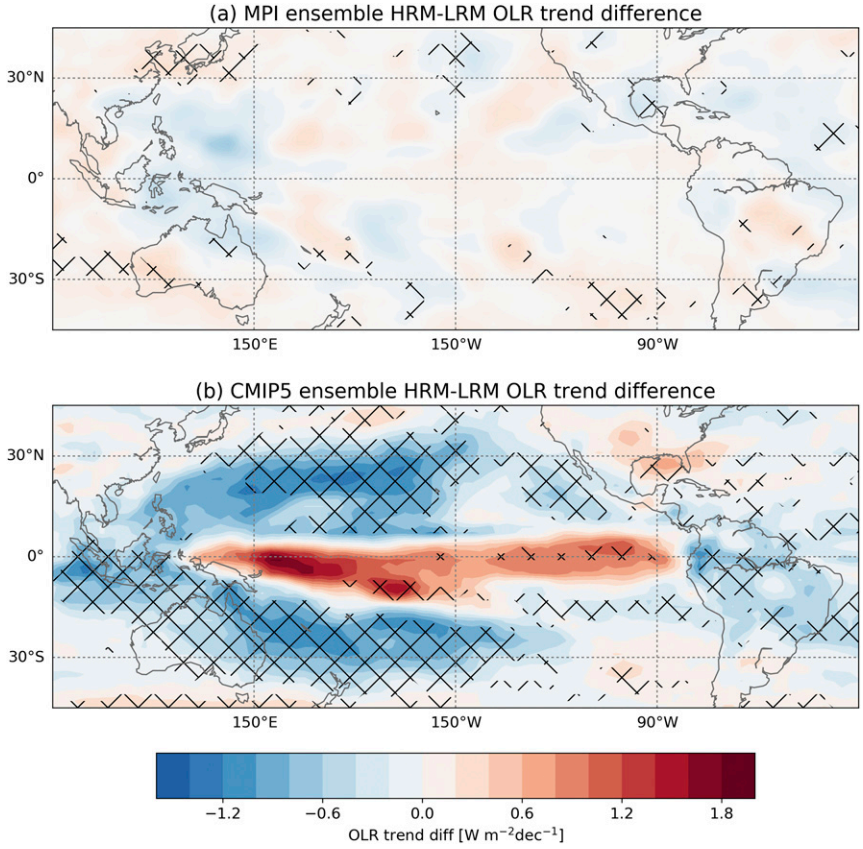

FIG. 6. Mean OLR trend difference between HRMs and LRMs for the (a) MPI ensemble and (b) the CMIP5 ensemble. The cross hatching shows the regions where the sign of the trend differs between LRMs and HRMs. Blue areas without hatching are where the models with less circulation slowdown (HRM) have a stronger increase in cloudiness (lower OLR) than the areas with a stronger circulation slowdown (LRM).

Maritime Continent and of the tropical Pacific. The LRM group (Fig. 5f) reveals a strong significant negative OLR trend to the east of the Maritime Continent. This is indicative of increasing cloudiness related to the intensification of convection in this region and the eastward shift of the ascending branch of the Pacific Walker cell. On the other hand, in Fig. 5h the HRM suggests only a small increase in cloudiness over the equatorial region of the Maritime Continent, but a strongly intensified cloudiness over its northern region, consistent with more active convection in the Pacific Walker cell. In the OLR trends in the HRM model, we also identify a pronounced southern branch of the ITCZ in the southwestern Pacific, which is nonexistent in the LRM models.

A similar picture to the differences in OLR trend between the LRM and HRM ensemble members emerges in the surface temperature change over the tropical Pacific (Fig. 7). The LRM ensemble members show an overall larger increase of surface temperature across the equatorial Pacific and, especially over the eastern Pacific, a pattern compatible with an El Niño state of the climate system and a slower Walker circulation. The temperature variation over the Maritime Continent is also smaller and more uniform in the HRMs than in the LRMs, consistent with a nonchanging or strengthening circulation (Figs. 5f,h).

This analysis of the relation between the changes in OLR over the tropical Pacific and the variation of the Walker Pacific cell dynamics shows that even if the detected variances of the circulation trends in the two ensembles are similar, the variability is caused by different factors. For the Walker circulation trends in the MPI ensemble, which are driven by internal variability, the patterns in OLR change are comparable (differing mostly in magnitude) between the runs projecting the most weakened circulation and the runs projecting the less-changing or strengthening circulation. On the other hand, the CMIP5 ensemble shows that a GCM with a strong decrease in the intensity of the Walker cell will

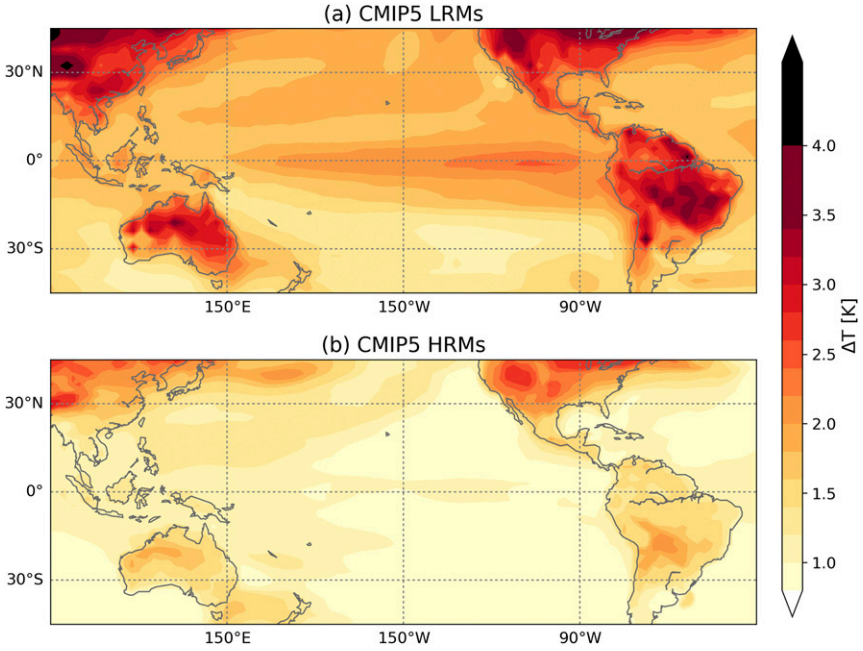

FIG. 7. Surface temperature change at the moment of CO_2 doubling in the 1pctCO2 experiment output, averaged for (a) the LRM and (b) the HRM CMIP5 models.

likely have a drier Maritime Continent, a significant eastward shift of the ascending branch of the cell, and a warmer eastern and central Pacific by CO_2 doubling than a GCM with a stronger circulation. It has been suggested by Bony et al. (2013) and Su et al. (2014) that these intermodel differences likely arise from the differences in the representation of small-scale moist processes, such as convection and clouds, and their interaction with the large-scale circulation.

4. Conclusions

This study investigates the robustness of a weaker Pacific Walker circulation under constant increase in CO_2 forcing and its sensitivity to natural variability, GCM configuration, and the chosen indexing method. The analysis was carried out on two ensembles of GCMs simulations of the CMIP5 1pctCO2 experiment setting: the MPI ensemble (based on slightly perturbed initial climate states) and the CMIP5 ensemble (consisting of distinct GCMs). Three simple indices were used for the computation of the Walker circulation intensity time series.

We find that, regardless of the ensemble and chosen indexing method, a weakening Pacific Walker cell is the most probable scenario for a transient CO_2 increase. The variance of this response is of comparable magnitude in the CMIP5 ensemble and the MPI ensemble, suggesting that the Walker circulation trend for the considered time period of 70–140 yr is as dependent on the initial climate state as on the model's physics. The comparison between the projection of mean surface temperature and circulation intensity change by the moment of CO_2 doubling shows much less variance in the former than in the latter, regardless of the ensemble. This difference seems to reflect the better understanding and simulation in GCMs of the thermodynamical changes than of the atmospheric circulation's response to increased forcing, a general point that has been argued by Shepherd (2014).

An index-only comparison between simulated Walker circulation changes must consider the variability and sensitivity of the index's base parameter to increased CO_2 concentration. The MSLP index is indicative of the intensity of the lower branch of the Pacific Walker cell and is highly sensitive to the internal variability of MSLP and the parameterization of boundary layer processes within the GCM. The ω_{500} and χ_{200} indices reveal a dependence on the cloud and convection parameterization of the climate model, as they represent the ascending branch and the upper-tropospheric branch of the cell, respectively. Therefore, a future study of the Walker circulation change in a specific climate experiment should not take into account the model's physical basis and parameterizations exclusively. The quantification of the circulation's intensity variation should also consider the sensitivity of the index's base parameter to various atmospheric processes and forcings.

This work was not aimed to identify the best index to represent the intensity of the Walker circulation. We considered widely accepted indices and showed that, although they relate to the same complex phenomenon, the Pacific Walker cell, the correlation between their time series is not large enough to ensure the same variance of the response. Also, because of these differences, in some GCMs the three indices suggest distinct changes of intensity. The analysis suggests that these indices are, in fact, each describing one distinct aspect of the complex Walker cell phenomenon. The three indices regarded in this study all use quasi surfaces, albeit at different altitudes and with focus on different parameters. The definitions of two indices (MSLP and ω_{500} indices) are based on fixed spatial boxes in the eastern and western Pacific. It is likely that a spatial change in the structure of the cell (e.g., a decreased zonal extent) would require an update of this preset parameter. Also, as seen in the mean piControl cross section of vertical velocity over the equatorial Pacific, there is significant variance in the representation of the Pacific Walker cell in the GCM, even in an unforced climate system. This result leads again to the possible need for adjusting the indices to each GCM and/or to the choice of indices that are not confined to a limited spatial box, as the MSLP and ω_{500} indices are. Another facet of the circulation change may be provided by an index describing the mass transport within the cell, which was beyond the scope of this study. Such an index, like the one based on zonal mass streamfunction, defined by Yu and Zwiers 2010), may give indication of both intensity and structural changes of the cell.

We ranked the MPI and CMIP5 ensemble members according to their Walker circulation response, and we investigated the differences between the model runs that project the strongest weakening of the Pacific Walker cell and those that project no change or the strengthening of the Walker cell. This revealed that the two groups are not obviously different in their representation of the mean Walker circulation in the control climate; the difference becomes apparent only upon forcing. The forcing also amplifies the intermodel differences caused by the distinct representations of the interaction between small- and large-scale atmospheric processes. An analysis of the OLR changes over the tropical Pacific in the two identified groups also revealed that a strong weakening of the Walker circulation will be associated with a drier Maritime Continent, an increased convection eastward from this region, and a warmer tropical Pacific in comparison to a strengthened circulation.

A secondary result of investigating the forced dynamical response of the Pacific Walker cell is the apparent robustness of its structural response—that is, the eastward shift of the ascending branch of the cell. This spatial response of the circulation may be detected in various indices as well as in basic climate elements, such as the pattern of OLR and surface temperature change across the tropical Pacific. This response to the warming climate may also partly explain the differences detected in the response of the Walker circulation: as two of the investigated indices are based on fixed boxes in the eastern and western Pacific, this shift of the ascending branch would impact the estimation of the MSLP and vertical velocity gradient across the Pacific.

Although the forced response, estimated from the ensemble mean, is a circulation slowdown, several individual ensemble members show a circulation strengthening even for quite long time periods. For CO_2 doubling during 70 years, 3–6 out of 28 CMIP5 ensemble members (depending on index) show a significant circulation speedup going against the ensemble mean trend; for CO_2 quadrupling during 140 years, still 3–5 out of 28 models show this. This result is not limited to the CMIP5 ensemble: even in the MPI ensemble, where spread is driven exclusively by natural variability, up to 15 out of 68 members show a significant strengthening of the circulation going against the forced response, for the 70-yr time period. Two ensemble members still show this for the 140-yr time period, although the significance of the trend is lower. Thus, the uncertainty introduced in the simulation of the Walker circulation change by the GCM configuration and the choice of index, as well as the insufficient understanding of the circulation's internal variability, affects the predictability of and the confidence in a weaker circulation under increased CO_2 forcing.

Acknowledgments. Elina Plesca was supported through the Cluster of Excellence CliSAP (EXC177), Universität Hamburg, funded through the German Science Foundation (DFG). Stefan A. Buehler was partially supported by DFG Research Group 1740 (contract BU2253/1-2), by BMBF project HD(CP)^2 (contracts O1LK1502B and O1LK1505D), and by the DFG HALO research program (contract BU2253/3-1). We acknowledge the Max Planck Institute for Meteorology, Hamburg, Germany, for creating and providing access to the output of the MPI-ESM-LR model ensemble. We thank the World Climate Research Programme's Working Group on Coupled Modelling, responsible for CMIP5, and the institutions responsible for the models listed in Table 1. The CMIP5 data were accessed through the German Climate Computing Centre (DKRZ) ESGF-CoG node. We also thank ECMWF for the ERA-Interim dataset, which was downloaded

from the ECMWF public data portal. We thank the three anonymous reviewers for their effort in revising this work and also Bjorn Stevens, Thorsten Mauritsen, and Thomas Birner for the constructive discussions about the findings of this study.

REFERENCES

Bayr, T., D. Dommenget, T. Martin, and S. B. Power, 2014: The eastward shift of the Walker circulation in response to global warming and its relationship to ENSO variability. *Climate Dyn.*, **43**, 2747–2763, doi:10.1007/s00382-014-2091-y.

Bony, S., G. Bellon, D. Klocke, S. Sherwood, S. Fermepin, and S. Denvil, 2013: Robust direct effect of carbon dioxide on tropical circulation and regional precipitation. *Nat. Geosci.*, **6**, 447–451, doi:10.1038/ngeo1799.

Chadwick, R., I. Boutle, and G. Martin, 2013: Spatial patterns of precipitation change in CMIP5: Why the rich do not get richer in the tropics. *J. Climate*, **26**, 3803–3822, doi:10.1175/JCLI-D-12-00543.1.

Cubasch, U., and Coauthors, 2001: Projections of future climate change. *Climate Change 2001: The Scientific Basis*, J. T. Houghton et al., Eds., Cambridge University Press, 526–582.

Davis, N., and T. Birner, 2016: Climate model biases in the width of the tropical belt. *J. Climate*, **29**, 1935–1954, doi:10.1175/JCLI-D-15-0336.1.

England, M. H., and Coauthors, 2014: Recent intensification of wind-driven circulation in the Pacific and the ongoing warming hiatus. *Nat. Climate Change*, **4**, 222–227, doi:10.1038/nclimate2106.

Gregory, J., and P. Forster, 2008: Transient climate response estimated from radiative forcing and observed temperature change. *J. Geophys. Res.*, **113**, D23105, doi:10.1029/2008JD010405.

Held, I. M., and B. J. Soden, 2006: Robust responses of the hydrological cycle to global warming. *J. Climate*, **19**, 5686–5699, doi:10.1175/JCLI3990.1.

IPCC, 2013: *Climate Change 2013: The Physical Science Basis*. Cambridge University Press, 1535 pp., doi:10.1017/CBO9781107415324.

Kociuba, G., and S. B. Power, 2015: Inability of CMIP5 models to simulate recent strengthening of the Walker circulation: Implications for projections. *J. Climate*, **28**, 20–35, doi:10.1175/JCLI-D-13-00752.1.

Ma, J., and S.-P. Xie, 2013: Regional patterns of sea surface temperature change: A source of uncertainty in future projections of precipitation and atmospheric circulation. *J. Climate*, **26**, 2482–2501, doi:10.1175/JCLI-D-12-00283.1.

Ma, S., and T. Zhou, 2016: Robust strengthening and westward shift of the tropical Pacific Walker circulation during 1979–2012: A comparison of 7 sets of reanalysis data and 26 CMIP5 models. *J. Climate*, **29**, 3097–3118, doi:10.1175/JCLI-D-15-0398.1.

Power, S. B., and G. Kociuba, 2011a: The impact of global warming on the Southern Oscillation Index. *Climate Dyn.*, **37**, 1745–1754, doi:10.1007/s00382-010-0951-7.

——, and ——, 2011b: What caused the observed twentieth-century weakening of the Walker circulation? *J. Climate*, **24**, 6501–6514, doi:10.1175/2011JCLI4101.1.

Shepherd, T. G., 2014: Atmospheric circulation as a source of uncertainty in climate change projections. *Nat. Geosci.*, **7**, 703–708, doi:10.1038/ngeo2253.

Su, H., J. H. Jiang, C. Zhai, T. J. Shen, J. D. Neelin, G. L. Stephens, and Y. L. Yung, 2014: Weakening and strengthening structures in the Hadley circulation change under global warming and implications for cloud response and climate sensitivity. *J. Geophys. Res. Atmos.*, **119**, 5787–5805, doi:10.1002/2014JD021642.

Tanaka, H., N. Ishizaki, and A. Kitoh, 2004: Trend and interannual variability of Walker, monsoon and Hadley circulations defined by velocity potential in the upper troposphere. *Tellus*, **56A**, 250–269, doi:10.3402/tellusa.v56i3.14410.

Taylor, K. E., R. J. Stouffer, and G. A. Meehl, 2012: An overview of CMIP5 and the experiment design. *Bull. Amer. Meteor. Soc.*, **93**, 485–498, doi:10.1175/BAMS-D-11-00094.1.

Vecchi, G. A., and B. J. Soden, 2007: Global warming and the weakening of the tropical circulation. *J. Climate*, **20**, 4316–4340, doi:10.1175/JCLI4258.1.

——, ——, A. T. Wittenberg, I. M. Held, A. Leetmaa, and M. J. Harrison, 2006: Weakening of tropical Pacific atmospheric circulation due to anthropogenic forcing. *Nature*, **441**, 73–76, doi:10.1038/nature04744.

Wang, C., 2002: Atmospheric circulation cells associated with the El Niño–Southern Oscillation. *J. Climate*, **15**, 399–419, doi:10.1175/1520-0442(2002)015<0399:ACCAWT>2.0.CO;2.

Yu, B., and F. W. Zwiers, 2010: Changes in equatorial atmospheric zonal circulations in recent decades. *Geophys. Res. Lett.*, **37**, L05701, doi:10.1029/2009GL042071.